RSC Advances

Synthesis of Pt-Rich@Pt-Ni Alloy Core-Shell Nanoparticles Using Halides

Journal:	*RSC Advances*
Manuscript ID:	RA-ART-11-2014-014095.R1
Article Type:	Paper
Date Submitted by the Author:	21-Dec-2014

Complete List of Authors:	Hwang, Eui-Tak; Soongsil University, Chemical Engineering Lee, Young-Woo; Soongsil University, Chemical and Environmental Engineering Park, Han-Chul; Soongsil University, Chemical Engineering Kwak, Da-Hee; Soongsil University, Soongsil University Kim, Da-Mi; Soongsil University, Chemical Engineering Kim, Si-Jin; Soongsil University, Chemical and Enviromental Engineering Kim, Min-Chul; Soongsil University, Chemical Engineering Lee, Jin-Yeon; Soongsil University, Chemical Engineering Lee, Seul; Soongsil University, Chemical Engineering Park, Kyung-Won; Soongsil University, Chemical Engineering

RSC Advances

RSCPublishing

ARTICLE

Synthesis of Pt-Rich@Pt-Ni Alloy Core-Shell Nanoparticles Using Halides

Eui-Tak Hwang, Young-Woo Lee, Han-Chul Park, Da-Hee Kwak, Da-Mi Kim, Si-Jin Kim, Min-Cheol Kim, Jin-Yeon Lee, Seul Lee, and Kyung-Won Park*

We demonstrated the synthesis of Pt-Ni alloy core-shell nanoparticles (NPs) via a one-pot thermal decomposition method, optimized by variation of the concentration of cetyltrimethylammonium chloride (CTAC) and reaction time. The samples prepared without CTAC and in 30 mM CTAC at 250 °C for 180 min exhibited the formation of single Pt-rich phases between metallic phases. With increasing CTAC concentrations (60-120 mM) at a constant temperature and time (250 °C for 180 min), the products contained both Pt-rich and Pt-Ni alloy phases, consisting of a Pt-rich core with a Pt-Ni alloy shell (Pt-rich@Pt-Ni), in contrast to the single Pt-rich phases prepared at low concentrations or in the absence of CTAC. As the reaction time increased from 10 to 180 min in 60 mM CTAC at 250 °C, the Pt-rich NPs were observed to grow in the initial stage, i.e. until a critical reaction time of 60 min, with subsequent formation of the Pt-Ni alloy phase on top of the as-formed Pt-rich NPs. The morphology and structure of the as-prepared NPs were characterized using TEM, EDX and XRD.

Introduction

Metallic nanostructures with a particularly large active surface area and a highly branched morphology have received much attention because of the fact that their morphology and composition can be adjusted to enhance catalytic,[1-11] magnetic,[12-14] and electrical[15-17] properties. For instance, Pt-based alloy nanoporous nanoparticles (NPs) such as Pt-Ni, Pt-Co, and Pt-Cu, having large surface areas and small pores, were synthesized via a facile chemical dealloying process using nanocrystalline alloys as precursors.[10] Porous single-crystalline Pd NPs of controllable sizes have been prepared by using a seed-mediated method in aqueous solutions with cetyltrimethyl-ammonium chloride (CTAC) as a stabilizing agent.[5] In particular, Pt-based core-shell NPs such as Au@Pt, Pt@Pd, and Pd@Pt have gained interest due to their excellent properties compared to monometallic nanostructures. Recently, the simultaneous reduction of multiple metal precursors with reducing agents in the presence of CTAC resulted in the formation of trimetallic Au@PdPt core-shell NPs with an octahedral Au core and a dendrite Pd-Pt alloy shell.[18] Furthermore, Au@Pd@Pt triple-layered core-shell NPs consisting of an Au core, Pd inner layer, and nanoporous Pt outer shell have also been synthesized, using a simple spontaneous method.[19,20]

However, for the preparation of core-shell alloy nanostructures, the use of a two-step seed-mediated method has considerable processing difficulties, resulting in formation of heterogeneous NPs. Therefore, there is a large need for the challenging creation of a facile one-pot method for formation of porous core-shell alloy nanostructures. Most metal NP synthesis methods in water or polar solvents have other additive ions including halides such as chloride, bromide, or iodide, which have a strong tendency to adsorb onto the metallic surfaces, affecting the corresponding surface energies.[21] Fundamental studies on the effects of additives on the growth kinetics of these reaction systems have investigated how the type of additive affects nanoparticle growth.[22]

Here, we suggested Pt-Ni nanostructures consisting of a Pt-rich core and a Pt-Ni alloy shell (Pt-rich@Pt-Ni), by means of a one-pot thermal decomposition method in the presence of CTAC in organic solution. The Pt-Ni core-shell NPs were prepared by varying the synthetic conditions such as CTAC concentration, reaction time, and type of halide, etc.

Experimental

Pt-rich@Pt-Ni NPs were prepared by means of a one-pot thermal decomposition method in the presence of CTAC as a capping agent. A mixture solution of 10 ml 1-octadecene (90%, Aldrich), 2 ml oleylamine (70%, Aldrich), 2 ml oleic acid

(65~88%, Aldrich), and 30-120 mM CTAC (25%, Aldrich) was prepared at 250 °C under a N_2 atmosphere. A metal salt solution of 0.0442 g $Pt(acac)_2$ (97%, Aldrich), 0.035 g $Ni(acac)_2$ (95%, Aldrich), 5 ml 1-octadecene, and 4 ml oleylamine was added to the mixture, and kept at 250 °C for different reaction times. For comparison, pure Pt NPs were prepared by means of a thermal decomposition method in the presence of CTAC without Ni salt. A metal salt solution of 0.0442 g $Pt(acac)_2$, 5 ml 1-octadecene, and 4 ml oleylamine was added to the mixture, and kept at 250 °C for 180 min. All resulting colloidal solutions were rapidly cooled down by pouring into 100 ml n-hexane (95%, SAMCHUN). The resulting products were collected and washed several times with ethanol (95%, SAMCHUN) using centrifugation. To completely remove the remaining surfactant after the reaction, the products were maintained in a 30 ml acetic acid solution (99.7%, SAMCHUN) at 80 °C for 12 h.[23] The final products were washed with ethanol several times and dried using an evaporator.

The morphology of the samples is characterized by field-emission transmission electron microscopy (FE-TEM) and high-angle annular dark-field scanning TEM (HAADF-STEM) using a Tecnai G2 F30 system operating at 300 kV. Energy dispersive X-ray spectroscopy EDX analysis of the samples was performed on an FE-TEM (Tecnai G2 F30 system). TEM samples were prepared by placing drops of the nanoparticle suspension dispersed in ethanol on a carbon-coated copper grid. For structural analysis of the catalysts, X-ray diffraction (XRD) analysis was carried out using a Bruker D2 PHASE system with Cu Kα source (λ= 0.15406 nm) radiation at 30 kV and 10 mA.

Results and discussion

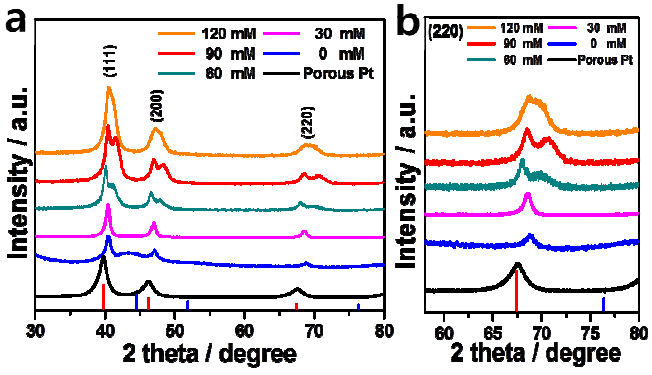

Fig. 1 Wide (a) and fine (b) scan XRD patterns of the as-prepared Pt-Ni NPs, prepared with varying CTAC concentrations at 250 °C for 180 min. The red and blue bars correspond to the reference peaks of Pt and Ni.

The samples were prepared via a thermal decomposition method at 250 °C for 180 min, with different concentrations of CTAC. In the case of pure Pt, the XRD peaks at 39.67, 46.15, and 67.48 corresponded to (111), (200), and (220), respectively, indicating a face-centered cubic (fcc) crystal structure. The samples prepared without CTAC and in 30 mM CTAC exhibited a higher XRD peak shift in the 2θ values compared to the typical polycrystalline Pt. Assuming a substitutional solid solution between Pt and Ni, the higher angle shift of the diffraction peak positions reveals a single Pt-rich phase formation between metallic phases.[24,25] However, it is surprising that with increasing CTAC concentration in the range of 60-120 mM, the products seemed to have overlapping

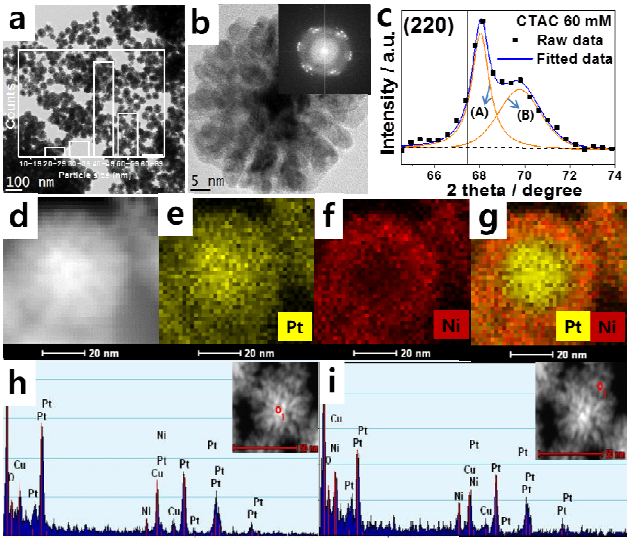

Fig. 2 FE-TEM (a) and HR-TEM (b) images, and fine scan XRD pattern (c) of Pt-rich@Pt-Ni prepared in the presence of 60 mM CTAC at 250 °C for 180 min. HAADF-STEM image and elemental mapping profiles (d)-(g) of a single Pt-rich@Pt-Ni NP. EDX spectra of the core (h) and shell (i) regions of a single Pt-rich@Pt-Ni NP.

XRD peaks relevant to Pt-based alloy phases in the overall diffraction range (Fig. 1(a)). In particular, (220) peaks for the products could be evidently distinguished by two peaks, implying that the products prepared at relatively high CTAC concentrations contained two Pt-Ni alloy phases, compared to those prepared at lower concentrations or in the absence of CTAC. Structural analysis of the sample prepared in the presence of 60 mM CTAC at 250 °C for 180 min was carried out, as shown in Fig. 2. The as-synthesized NPs had an average size of 45.7 nm and a very dark contrast at the center of the nanodendrites, indicating that the NPs had three-dimensional structures (Fig. 2(a and b)).[26-29] The inset of Fig. 2(b) exhibited a polycrystalline structure of the NPs as also confirmed in the XRD data. Furthermore, as indicated in Fig. 2(c), the XRD peak of the NPs could be evidently fitted by two peaks (denoted as A and B, respectively).[30] On the basis of the Vegard's law of $d_{Pt-Ni} = x \cdot d_{Pt} + (1-x) \cdot d_{Ni}$, the Pt:Ni atomic ratios estimated from the diffraction peaks of A and B were 94:6 and 74:26, respectively.[31,32] The XRD analysis indicated that the Pt-

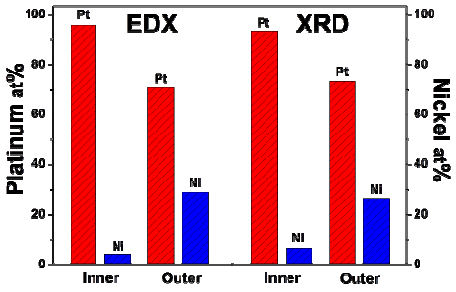

Fig. 3 Comparison of the elemental compositions of Pt and Ni for the Pt-rich@Pt-Ni prepared in the presence of 60 mM CTAC at 250 °C for 180 min.

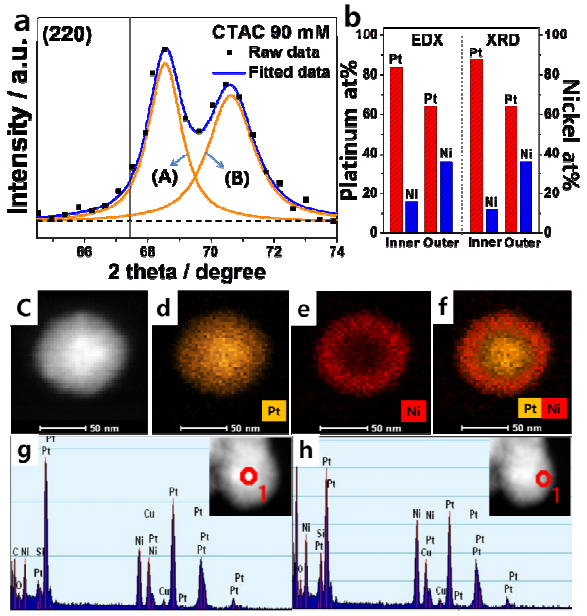

Fig. 4 Fine scan XRD pattern (a) of Pt-rich@Pt-Ni prepared in the presence of 90 mM CTAC at 250 °C for 180 min. (b) Comparison of the elemental compositions of Pt and Ni for the Pt-rich@Pt-Ni prepared in the presence of 90 mM CTAC at 250 °C for 180 min. HAADF-STEM images and elemental mapping profiles (c-f) of a single Pt-rich@Pt-Ni NP. EDX spectra of the core (g) and shell (h) regions in the Pt-rich@Pt-Ni NP.

Ni NPs contained two distinct phases with different elemental compositions of Pt and Ni. The HAADF-STEM and elemental mapping images of a single NP were characterized, as shown in Fig. 2(d-g). The elemental mapping of Pt and Ni obtained by HAADF-STEM-EDX revealed that the as-prepared sample held two different Pt:Ni ratios, in the inner and outer regions.

Furthermore, the point EDX analysis of the single NP supported the existence of two elemental compositions of Pt:Ni, i.e. (96:4) and (71:29) in the inner and outer regions, respectively (Fig. 2(h and i)). The EDX data demonstrated that the Pt-Ni NPs contained two distinct phases with different elemental compositions of Pt and Ni, which is in good agreement with the XRD analysis (Fig. 3).

The samples prepared in the presence of 90 and 120 mM CTAC at 250 °C for 180 min were also characterized by XRD, HAADF-STEM, and EDX. In the case of the sample prepared with 90 mM CTAC, the atomic ratios of Pt:Ni estimated from the XRD diffraction peaks of A and B were 88:12 and 64:36, respectively, corresponding to the elemental compositions of Pt:Ni = (84:16) and (66:34) in the inner and outer regions, respectively, measured by EDX (Fig. 4). In the case of the sample prepared with 120 mM CTAC, the Pt:Ni atomic ratios were estimated to be 87:13 and 73:27, respectively, corresponding to elemental compositions of Pt:Ni = (81:19) and (72:28) in the inner and outer regions, respectively, measured by EDX (Fig. 5). Comparing the data from XRD and EDX, it can be inferred that NPs consisting of a Pt-rich core with a Pt-Ni alloy as a shell (Pt-rich@Pt-Ni) can be prepared by a one-pot process at relatively high concentrations of CTAC.

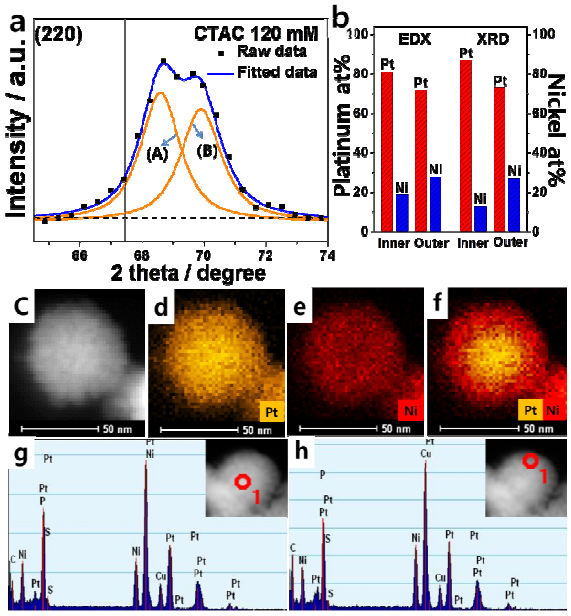

Fig. 5 Fine scan XRD pattern (a) of Pt-rich@Pt-Ni prepared in the presence of 120 mM CTAC at 250 °C for 180 min. (b) Comparison of the elemental compositions of Pt and Ni for the Pt-rich@Pt-Ni prepared in the presence of 120 mM CTAC at 250 °C for 180 min. HAADF-STEM images and elemental mapping profiles (c-f) of a single Pt-rich@Pt-Ni NP. EDX spectra of the core (g) and shell (h) regions in the Pt-rich@Pt-Ni NP.

To demonstrate the effect of reaction time on the growth of the Pt-rich@Pt-Ni NPs, the samples were synthesized in 60 mM CTAC at 250 °C for various reaction times. The XRD patterns of the NPs grown for 10~60 min exhibited a slightly higher angle shift of the diffraction peak positions compared to polycrystalline Pt with an fcc structure, indicating the presence of a single Pt-rich phase with an average composition of Pt:Ni = 93:7 (Fig. 6). Following 100 min growth, the Pt-Ni NPs displayed XRD peaks fitted by two phases with different

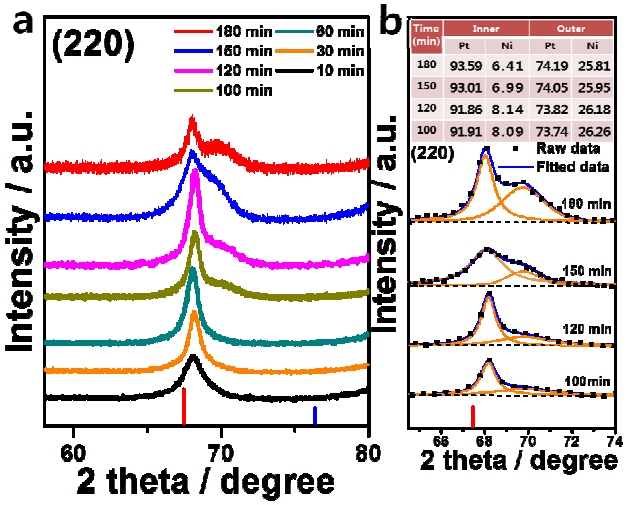

Fig. 6 Wide (a) and fine (b) scan XRD patterns of the as-prepared Pt-Ni NPs prepared in the presence of 60 mM CTAC at 250 °C for varying reaction times. The red and blue bars in Fig. 6 correspond to the reference peaks of Pt and Ni.

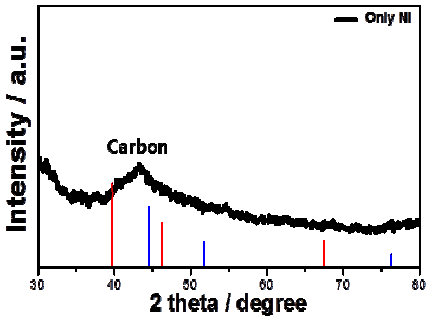

Fig. 7 XRD pattern of the product prepared from Ni salt solution with 60 mM CTAC in the absence of Pt salt at 250 °C for 180 min.

compositions of Pt and Ni. The Pt:Ni atomic ratios estimated from the left-side and right-side diffraction peaks were 92:8 and 74:26, respectively. After growth for 180 min, the Pt-Ni NPs also showed two Pt-based phases corresponding to A and B with Pt:Ni = 94:6 and 72:28, respectively. In synthetic conditions for the Pt-Ni NPs, such as 60 mM CTAC and 250 °C,

the Pt-rich phases form in the initial stage until a critical reaction time, after which the Pt-Ni alloy phases form. By considering both the effects of CTAC concentration and reaction time, it was concluded that the Pt-rich@Pt-Ni NPs can be formed at a critical CTAC concentration (> 60 mM) during a reactions occurring over a particular period of time (> 100 min).

It is notable that the standard reduction potential of Pt^{2+} into Pt^{o} is much higher than that of Ni^{2+} into Ni^{o}, thus implying that the formation of Pt nuclei is more spontaneous than that of Ni nuclei.[18-20,33] As indicated in Fig. 7, no nickel metallic phase (Ni^{o}) was formed during the synthesis in Ni salt solution with CTAC in the absence of Pt. However, it was surprising that despite the difference in the standard reduction potential of metal salts, Pt^{2+} and Ni^{2+} could be co-reduced to zerovalent atoms. Recently, Li and co-workers reported that Ni^{2+} could be co-reduced to zerovalent atoms in the presence of noble metals such as Pt^{2+} by noble-metal-induced reduction (NMIR) effect.[34-36] It would be challenging to completely understanding of the role of the chloride in the synthesis of Pt-rich@Pt-Ni NPs, because of various halide-metal crystal and halide-metal ion interactions. However, Murphy and Haas suggested that the

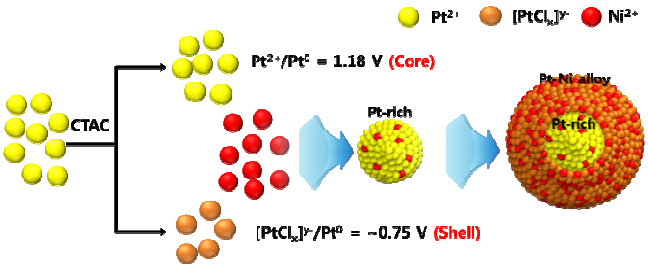

Fig. 8 Schematic growth mechanism of the Pt-rich@Pt-Ni NPs cntanning Pt^{2+} and $PtCl_x^{y-}$ with different reduction pathways.

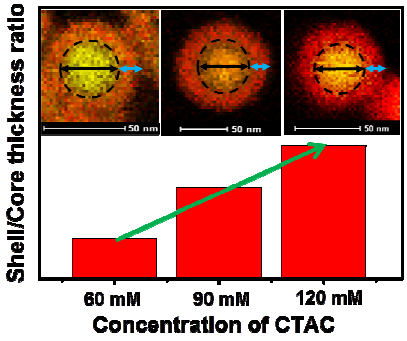

Fig. 9 Shell/core thickness ratio of the Pt-rich@Pt-Ni NPs with different CTAC concentration

interaction could change the reduction potential of the metal ion forming halide-metal complex with the influence of the halide concentration.[21,37] In our study, the reduction process of $[PtCl_x]^{y-}/Pt^{o}$ in the presence of CTAC could be accompanied with Pt^{2+}/Pt^{o}. At low concentrations or in the absence of CTAC, the Pt-Ni NPs with single Pt-rich phases might be formed by the process of Pt^{2+}/Pt^{o} reduction, with relatively high reduction potential. On the other hand, at relatively high CTAC concentrations, two completely different reduction pathways of both Pt^{2+}/Pt^{o} and $[PtCl_x]^{y-}/Pt^{o}$ with NMIR effect can result in two Pt-Ni alloy phases in the Pt-Ni NPs (Fig. 8). However, one fundamental question that Pt-Ni NPs consisting of a Pt-rich core and a Pt-Ni alloy as a shell could be prepared by a one-pot process at relatively high concentrations of CTAC is still remained. Haas et al. reported metal-halide complex could be formed in the presence of CTAB and the amount of complex was increased with CTAB concentration.[37] Also, in the present study, Pt-Cl complex (such as $PtCl_x^{y-}$) can be formed by CTAC and the amount of complex is increased with CTAC concentration. As a result, our synthetic system contains two types of Pt precursors such as Pt^{2+} and $PtCl_x^{y-}$, which might be reduced through two different reduction pathways as follows:

$$Pt^{2+} + 2e^{-} \rightarrow Pt \qquad E^{o} = 1.18\ V \qquad (1)$$

$$PtCl_x^{y-} + ze^{-} \rightarrow Pt + xCl^{-} \qquad E^{o} = \sim 0.75\ V \qquad (2)$$

In the synthetic system containing Pt2+ and $PtCl_x^{y-}$, Pt^{2+} can be firstly reduced with Ni forming a Pt-rich core in Pt-Ni NPs (Eq.(1)). Next, $PtCl_x^{y-}$ can be reduced with Ni at the lower reduction potential (Eq.(2)) forming a Pt-Ni alloy shell in Pt-Ni NPs. However, as shown in Fig. 9, the ratio of Pt-Ni alloy shell to Pt-rich core in Pt-Ni NPs was increased with CTAC concentration. This means that the portion of Pt-Ni alloy shell in Pt-Ni NPs is increased during the synthetic process with a higher CTAC concentration. Thus, $PtCl_x^{y-}$ formed by CTAC might facilitate the reduction of Ni compared to Pt^{2+}.

Furthermore, to confirm the effect of chlorine as a halogen agent on the formation of Pt-rich@Pt-Ni NPs, the sample was synthesized in the presence of 0.5 M HCl as a halogen source, instead of CTAC, at 250 °C for 180 min. From the XRD patterns of the product, the Pt:Ni atomic ratios for the diffraction peaks of A and B were determined to be 93:7 and 84:16, respectively (Fig. 10(a)). The XRD analysis indicated that the Pt-Ni NPs also contained two distinct Pt-Ni alloy phases with different elemental compositions of Pt and Ni. The HAADF-STEM and elemental mapping images of a single NP were characterized, as indicated in Fig. 10(b-e), revealing that the as-prepared sample held two different Pt:Ni ratios between the core and shell regions. Furthermore, the point EDX analysis of the sample supported two phase compositions of Pt:Ni, i.e. (92:8) and (85:15) in the inner and outer regions, respectively (Fig. 10(f and g)). By comparing the XRD and EDX data, it was found that the Pt-Ni NPs synthesized in the presence of HCl consisted of a Pt-rich phase as a core with a Pt-Ni alloy shell, which is in accordance with the Pt-Ni NPs synthesized in the presence of CTAC under the same conditions. This demonstrates that Cl sources from cetyltrimethylammonium chloride and hydrochloric acid can play a key role in the formation of Pt-rich@Pt-Ni NPs. Also, to investigate the effect of bromine as one of halogen agents on the formation of Pt-rich @Pt-Ni NPs, the samples were prepared in the presence of cetyltrimethylammonium bromide (CTAB) and HBr as a halogen source, respectively, instead of CTAC, at 250 °C for 180 min. By comparing the XRD and EDX data, it was found that the Pt-Ni NPs synthesized in the presence of CTAB and HBr consisted of Pt-rich cores and Pt-Ni alloy shells, which is in accordance with the Pt-Ni NPs synthesized in the presence of CTAC under the same conditions (Fig. 11 and 12). This suggests that Br sources from CTAB and HBr as well as Cl sources from CTAC and HCl can play a key role in the formation of Pt-rich@Pt-Ni NPs.

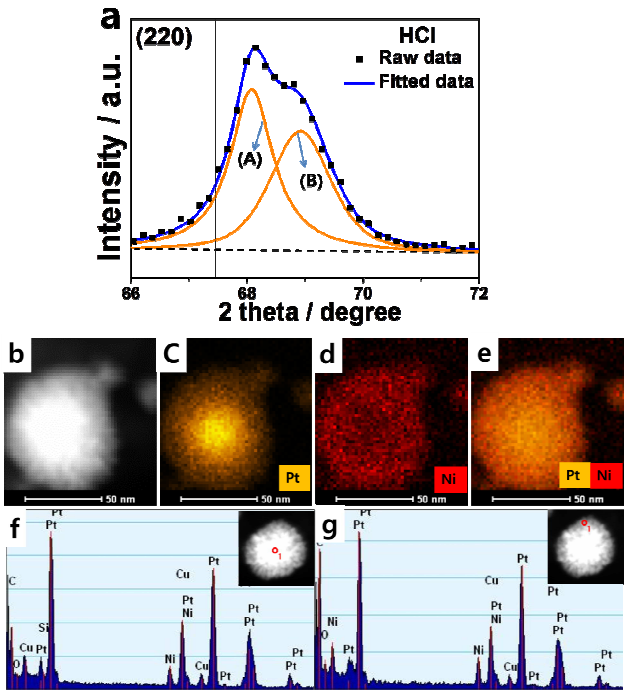

Fig. 10 (a) Fine scan XRD pattern of the Pt-Ni NPs prepared in 0.5 M HCl at 250 °C for 180 min. HAADF-STEM image and elemental mapping profiles (b-e) of a single Pt-Ni NP. EDX spectra of the core (f) and shell (g) regions in the Pt-Ni NP.

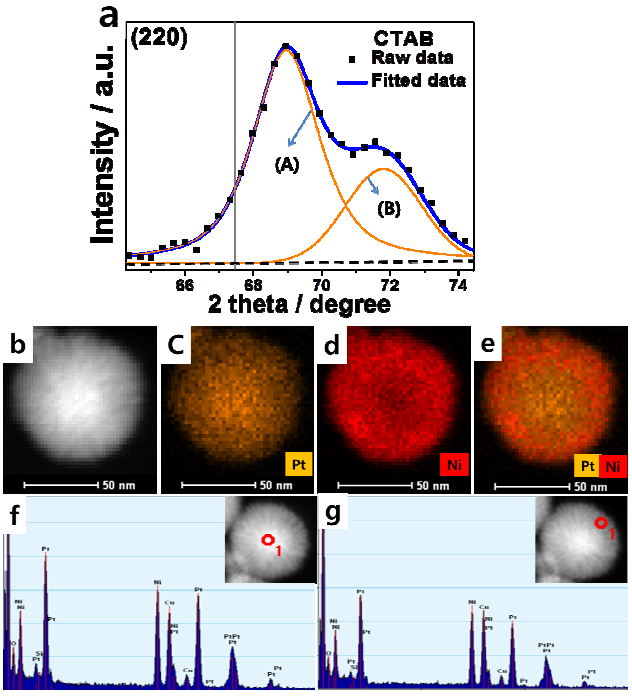

Fig. 11 Fine scan XRD pattern (a) of Pt-Ni NPs prepared in the presence of 60 mM CTAB at 250 °C for 180 min. HAADF-STEM images and elemental mapping profiles (b-e) of a single Pt-Ni NP. EDX spectra of the core (f) and shell (g) regions in the Pt-Ni NP.

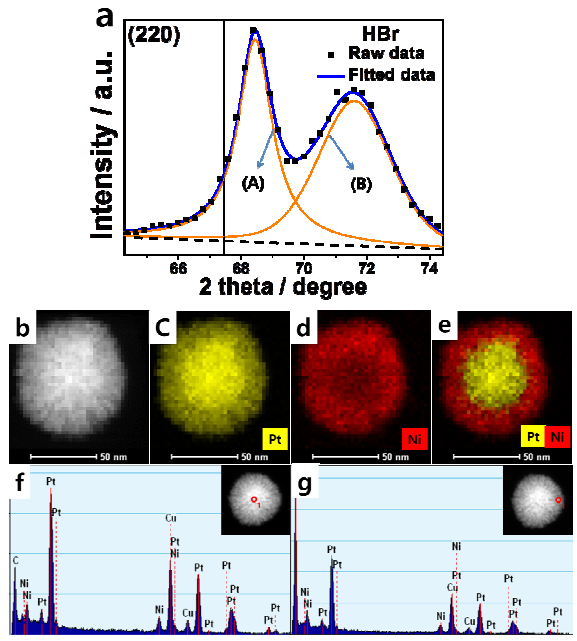

Fig. 12 Fine scan XRD pattern (a) of Pt-Ni NPs prepared in the presence of 0.5 M HBr at 250 °C for 180 min. HAADF-STEM images and elemental mapping profiles (b-e) of a single Pt-Ni NP. EDX spectra of the core (f) and shell (g) regions in the Pt-Ni NP.

Conclusions

In summary, we demonstrated the synthesis of Pt-Ni NPs by means of a one-pot thermal decomposition method in the presence of different CTAC concentrations, for different reaction times. In particular, the Pt-rich@Pt-Ni NPs consisting of a Pt-rich phase as a core with a Pt-Ni alloy shell could be prepared in relatively high CTAC concentrations under sufficient reaction times. In the early stages of the thermal decomposition process, at over critical values of both CTAC concentration and reaction time, the nucleation of Pt may occur dominantly in the core of the NPs compared to the Ni nucleation, resulting in the formation of a Pt-rich phase in the core of the NPs until a critical reaction time, after which the Pt-Ni alloy phases form. In the synthetic system containing Pt^{2+} and $PtCl_x^{y-}$, Pt^{2+} might be reduced with Ni forming a Pt-rich core, and then $PtCl_x^{y-}$ might be reduced with Ni at a lower reduction potential forming a Pt-Ni alloy shell in Pt-rich@Pt-Ni NPs. These NPs might be able to be used to improve the catalytic activities of hydrogenation or oxygen reduction reaction due to the change of the surface electronic structure.

Acknowledgements

This work was supported by the National Research Foundation of Korea Grant funded by the Korean Government (NRF-2013R1A1A2012541).

Notes and references

Department of Chemical Engineering, Soongsil University, Seoul 156743,
Republic of Korea. E-mail: kwpark@ssu.ac.kr; Fax: +82-2-812-5378;
Tel: +82-2-820-0613

1 B. Lim, M. Jiang, P. H. C. Camargo, E.C. Cho, J. Tao, Y. Zhu, Y. Xia, *Science*, 2009, **324**, 1302-1305.
2 S. E. Skrabalak, J. Chen, Y. Sun, X. Lu, L. Au, C. M. Cobley, Y. Xia, *Acc. Chem. Res.*, 2008, **41**, 1587-1595.
3 Y. He, N. Zhang, Q. Gong, Z. Li, J. Gao, H. Qiu, *Mater. Chem. Phys*., 2012, **134**, 585-589.
4 J. Watt, S. Cheong, M. F. Toney, B. Ingham, J. Cookson, P. T. Bishop, R. D. Tilley, *ACS Nano*, 2009, **4**, 396-402.
5 F. Wang, C. Li, L.-D. Sun, C.-H. Xu, J. Wang, J. C. Yu, C.-H. Yan, *Angew. Chem. Int. Ed*., 2012, **51**, 4872-4876.
6 B. Lim, M. Jiang, T. Yu, P. H. C. Camargo, Y. Xia, *Nano Res*., 2010, **3**, 69-80.
7 L. Chen, H. Guo, T. Fujita, A. Hirata, W. Zhang, A. Inoue, M. Chen, *Adv. Funct. Mater*., 2011, **21**, 4364-4370.
8 Z. Yin, H. Zheng, D. Ma, X. Bao, *J. Phys. Chem*., 2009, **113**, 1001-1005.
9 W. Wang, D. Wang, X. Liu, Q. Peng, Y. Li, *Chem. Commun*., 2013, **49**, 2903-2905.
10 D. Wang, P. Zhao, Y. Li, *Sci. Rep*., 2011, **1**, 37.
11 D.-J. Guo, Y. Ding, *Electroanalysis*, 2012, **24**, 2035-2043.
12 H.-T. Zhang, J. Ding, G.-M. Chow, *Langmuir*, 2008, **24**, 375-378.
13 M. Kurmoo, *Chem. Soc. Rev*., 2009, **38**, 1353-1379.
14 B. V. Harbuzaru, A. Corma, F. Rey, P. Atienzar, J. L. Jorda, H. Garcia, D. Ananias, L. D. Carlos, J. Rocha, *Angew. Chem. Int. Ed*., 2008, **47**, 1080-1083.
15 B. Lim, Y. Xia, *Angew. Chem. Int. Ed*., 2011, **50**, 76-85.
16 J. Chen, F. Saeki, B. J. Wiley, H. Cang, M. J. Cobb, Z.-Y. Li, L. Au, H. Zhang, M. B. Kimmey, X. Li, Y. Xia, *Nano Lett*., 2005, **5**, 473-477.
17 B. C. Tappan, S. A. Steiner, E. P. Luther, *Angew. Chem. Int. Ed*., 2010, **49**, 4544-4565.
18 S. W. Kang, Y. W. Lee, Y. Park, B.-S. Choi, J. W. Hong, K.-H. Park, S. W. Han, *ACS Nano*, 2013, **9**, 7945-7955.
19 L. Wang, Y. Yamauchi, *J. Am. Chem. Soc*., 2010, **132**, 13636-13638.
20 L. Wang, Y. Yamauchi, *Chem. Mater*., 2011, **23**, 2457-2465.
21 S. E. Lohse, N. D. Burrows, L. Scarabelli, L. M. Liz-Marzán, C. J. Murphy, *Chem. Mater*., 2014, **26**, 34-43.
22 A. P. LaGrow, B. Ingham, M. F. Toney, R. D. Tilley, *J. Phys. Chem. C*, 2013, **117**, 16709-16718.
23 S.-I. Choi, R. Choi, S. W. Han, J. T. Park, *Chem. Commun*., 2010, **46**, 4950-4952.
24 Y. Yamauchi, S. S. Nair, T. Momma, T. Ohsuna, T. Osaka, K. Kuroda, *J. Mater. Chem*., 2006, **16**, 2229-2234.
25 Y.-W. Lee, B.-Y. Kim, K.-H. Lee, W.-J. Song, G. Cao, K.-W. Park, *Int. J. Electrochem. Sci*., 2013, **8**, 2305-2312.
26 X. W. Lou, C. Yuan, L. A. Archer, *Chem. Mater*., 2006, **18**, 3921-3923.
27 J. Yuan, W.-N. Li, S. Gomez, S. L. Suib, *J. Am. Chem. Soc*., 2005, **127**, 14184-14185.
28 B. Liu, H. C. Zeng, *J. Am. Chem. Soc*., 2004, 126, 8124-8125.
29 L. Wang, C. Hu, Y. Nemoto, Y. Tateyama, Y. Yamauchi, *Cryst. Growth Des*., 2010, **10**, 3454-3460.
30 J. Xu, G. Liu, J. Li, X. Wang, *Electrochim. Acta*, 2012, 59, 105-112.
31 A. V. G. Chizmeshya, M. R. Bauer, J. Kouvetakis, *Chem. Mater*., 2004, **15**, 2511-2519.
32 Y.-W. Lee, A.-R. Ko, D.-Y. Kim, S.-B. Han, K.-W. Park, *RSC Adv.*, 2012, **2**, 1119-1125.
33 D. R. Lide, CRC Handbook of Chemistry and Physics, 85th ed., *CRC Press*: Boca Raton, Florida, 2005.
34 D. Wang, Y. Li, *J. Am. Chem. Soc*., 2010, **132**, 6280-6281.
35 D. Wang, Q. Peng, Y. Li, *Nano Res*., 2010, **3**, 574-580.
36 D. Wang, Y. Li, *Adv. Mater*., 2011, **23**, 1044-1060.
37 I. Haas, A. Gedanken, *Chem. Mater*., 2006, **18**, 1184-1189.

